Reproducible DNA Thin Films Prepared by Laser Molecular Beam Deposition for Water Detection

Xuechen Shen[1,2*], Tomohiro Murata[1*], Shuai Liu[3], Kosuke Minami[4], Genki Yoshikawa[4,5], Nobuyuki Matsuki[3*], Katsuhiko Ariga[1,2*]

[1] Department of Advanced Materials Science, Graduate School of Frontier Sciences, The University of Tokyo, 5-1-5 Kashiwanoha, Kashiwa, Chiba 277-8561, Japan
[2] World Premiere International (WPI) Research Center for Materials Nanoarchitectonics (MANA), National Institute for Materials Science (NIMS), 1-1 Namiki, Tsukuba, Ibaraki 305-0044, Japan
[3]Department of Electrical, Electronics and Information Engineering, Faculty of Engineering, Kanagawa University, 3-27-1 Rokakubashi, Kanagawa-ku, Yokohama, Kanagawa 221-8686, Japan
[4]Research Center for Functional Materials, National Institute for Materials Science (NIMS), 1-1 Namiki, Tsukuba, Ibaraki 305-0044, Japan
[5]Materials Science and Engineering, Graduate School of Pure and Applied Science, University of Tsukuba, 1-1-1 Tennodai, Tsukuba, Ibaraki 305-8571, Japan

E-mail: 2631202228@edu.k.u-tokyo.ac.jp (X. Shen), t.murata20s@ams.k.u-tokyo.ac.jp (T. Murata), ARIGA.Katsuhiko@nims.go.jp (K. Ariga), matsuki@kanagawa-u.ac.jp (N. Matsuki)



Xuechen Shen
Xuechen Shen received his BASc in Engineering Science and MASc in Mechanical Engineering from the Faculty of Engineering at The University of Toronto. He has been pursuing Ph.D. studies since 2021 at the Department of Advanced Materials Science, Graduate School of Frontier Sciences at the University of Tokyo, doing research on fabrication of DNA thin films using laser deposition, and the resulting damage from the process.



Tomohiro Murata
Tomohiro Murata received his B.S. from the Department of Physics, Faculty of Science, Hokkaido University in 2018 and his M.S. from the Graduate School of Biomedical Science and Engineering from the same institute in 2020. He received a PhD in Science in 2023 from the Department of Advanced Materials Science, Graduate School of Frontier Sciences at the University of Tokyo. Currently, he is working as a postdoctoral researcher at the University of Tokyo. His current research focuses on achieving reliable fabrication and environmental stability of organic semiconductors toward high-performance sensing applications.



Katsuhiko Ariga
Katsuhiko Ariga received his Ph.D. degree from the Tokyo Institute of Technology in 1990. He joined the National Institute for Materials Science (NIMS) in 2004 and is currently the leader of the Supermolecules Group and principal investigator of the World Premier International (WPI) Research Centre for Materials Nanoarchitectonics (MANA), NIMS. He is also appointed as a professor at the University of Tokyo.

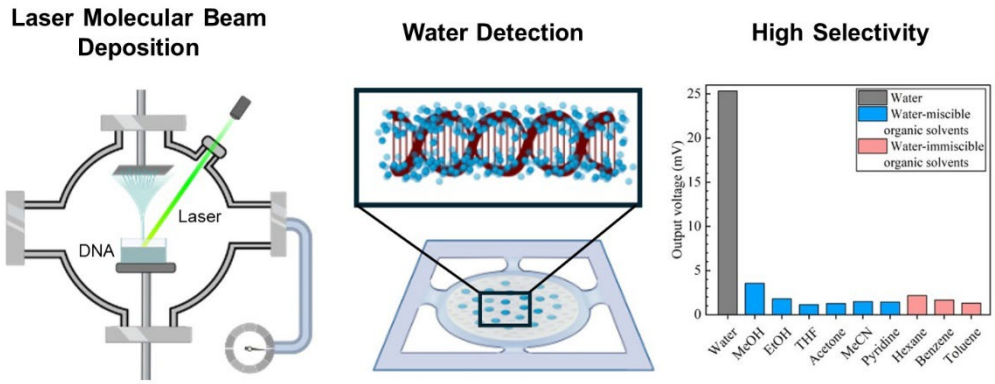


Nobuyuki Matsuki
Nobuyuki Matsuki received his Ph.D. degree from Tokyo Institute of Technology, Tokyo, Japan, in 2000. He worked as a post-doctoral researcher at several research institutes in Japan and abroad until 2008, then joined Gifu University as an assistant professor. From 2015 to the present, he has been an associate professor at Kanagawa University. His current research interests include development of thin solid films for electronics and photovoltaics.

Abstract
Reliable, accurate, and quick detection of trace amounts of water is crucial in food, beverage, pharmaceutical, and chemical industries. We previously developed a highly sensitive and selective water sensor surpassing the industry standard Karl Fischer titration in simplicity and efficiency. Here, we present laser molecular beam deposition (LMBD) fabrication of the water sensor, as an approach for mass-production of standardized and consistent units. The LMBD-fabricated sensor demonstrates altered morphology, but the sensor maintains high sensitivity and selectivity for detecting water.

Keywords: laser deposition, membrane-type surface stress sensor, water detection

Graphical Abstract



Introduction

The detection and quantification of trace amounts of water in organic solvents is critical in important industries including chemistry, pharmaceuticals, food and beverage, petrochemicals, and electronics[1–3]. The state of the art for water detection has been dominated by volumetric and coulometric Karl Fischer (KF) titration techniques for decades[2,4,5]. KF titration techniques are fast (<2 min) and accurate (±5%), but there are also limitations such as inability to monitor water content in real time and sensitivity to atmospheric moisture, as well as drawbacks such as requiring reagent adjustments based on the sample, careful yet quick handling to minimize moisture, and preparation time in advance[2].

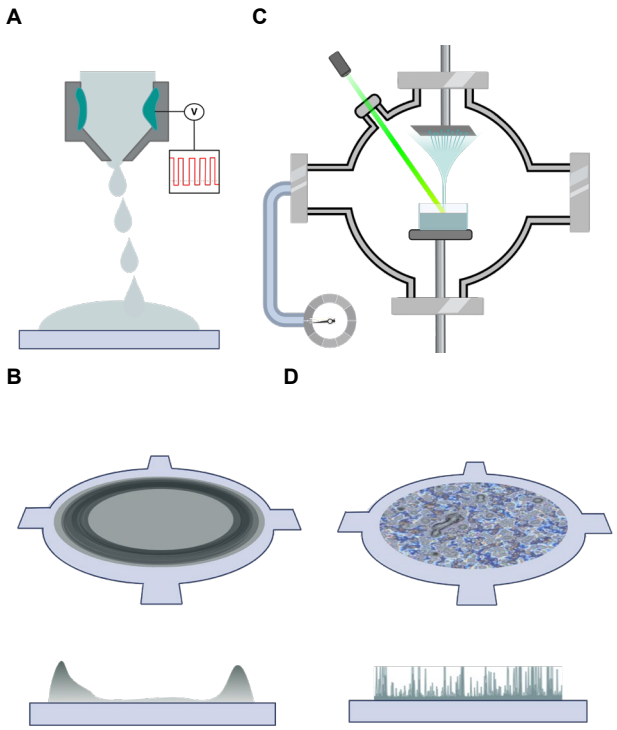


Fig. 1. **(A)** Previous fabrication approach: inkjet spotting of DNA in solution. **(B)** Resulting DNA thin films with limited reproducibility due to small perturbations in evaporation mechanics and slight in-solution inhomogeneities (top and side views). **(C)** Current fabrication approach: LMBD fabrication in a physical vapor deposition process with controlled pressure and temperature. **(D)** Resulting stochastic DNA film with macroscale batch consistency and sensing performance (top and side views).

Some alternative approaches have been explored, which include colorimetry and fluorometry[6,7], electrochemistry[8], and nuclear magnetic resonance[9]. However, these solutions have limitations of their own such as low sensitivity, insufficiencies in probe materials, and requirement of expensive equipment.

DNA is a biomolecule with strong interactions with water molecules attributed to charged groups in DNA backbone and nucleobases[10–12]. Consequently, the application of DNA as a receptor material for nanomechanical sensing yielding extremely low limit of detection (LoD) for trace amounts of water has been reported[13,14].

Murata et al. fabricated a DNA thin film by inkjet-spotting DNA dissolved in water onto a nanomechanical sensor (Fig. 1A). The DNA film adsorbs water and swells, causing the nanomechanical sensor to deform, and transduce the deformation into an electrical signal through piezoresistivity. In response to water vapor, the sensor demonstrated a response time within 30 s and a low limit of detection of 1.7×10^{-5}% relative humidity (RH). Furthermore, the sensor demonstrated high selectivity for water in a wide range of organic solvents at the parts-per-billion level[14]. Additionally, the sensor monitors moisture in real time and demonstrates portability, reusability, and ease of handling.

Nevertheless, the sensor had some limitations owing to its fabrication approach. Inkjet-based solution-processing causes inconsistencies between batches due to fluid dynamics while drying. Faster evaporation at the edges pulls more fluid outward via capillary flow, driving particles to the perimeter, in a phenomenon known as the coffee ring effect (Fig. 1B) [15–17]. Marangoni flow, caused by surface tension gradients, can either reinforce or suppress the coffee ring effect depending on solvent composition, temperature

gradients, and surfactants or impurities[18,19]. Consequently, the fabrication process becomes sensitive to slight fluctuations in ambient conditions, droplet impact and spreading dynamics, solution age and homogeneity, and drying time[20].

In the next study, Murata et al. used continuous infrared (IR) laser molecular beam deposition (LMBD) to fabricate a DNA thin film of controllable, nanometer thickness (as low as 26 nm), with a nanoscale surface roughness of 7.4 nm[21]. LMBD sublimates a target material onto a substrate using a high-energy laser beam in a physical vapor deposition process[21–24]. However, the high-energy laser beam exorbitantly damaged the phosphate backbone, diminishing the DNA film's ability to intercalate and thereby detect water, as well as making it more sensitive to methanol.

Aiming to achieve improved reproducibility of the DNA-thin-film water sensor while maintaining its water-sensitive features, we present our current investigation into LMBD fabrication using a pulsed visible laser (Fig.1C). In addition to the weaker energy of a short, single pulse of visible laser being less damaging, we found success processing DNA by freezing samples (-76 °C at 4 × 10^{-4} Pa vacuum) to partially attenuate the laser energy and inhibit structural damage[21,25]. Furthermore, the process occurs in a high vacuum, so ambient conditions are well-controlled, and molecular-scale perturbations are suppressed (Fig. 1D).

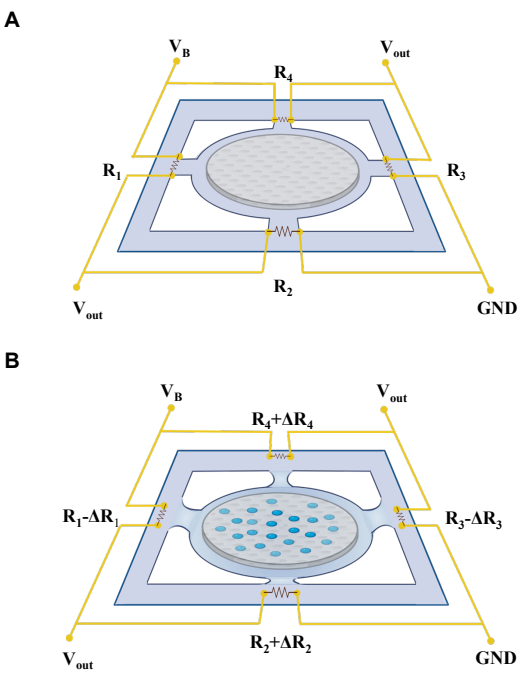


Fig. 2. The DNA-thin film deposited through LMBD becomes a receptor material on the circular membrane of the MSS **(A)** before exposure to water; **(B)** after exposure to water vapor, molecules are intercalated into the DNA film. Resulting deformation in the DNA film generates surface stress on the membrane, causing piezoresistor-embedded lever beams to change in resistance.

To transduce the adsorption of water to the DNA thin-film into an electrical signal, we continue the use of the Membrane-type Surface stress Sensor (MSS) from the previous study[14]. The MSS is a promising sensing platform for detecting trace amounts of molecules in the vapor phase, as it is an optimized structure for silicon-based nanomechanical sensing. Its fabrication process and working principle have been detailed in other studies[26–29], but we will also elaborate on its structure and operation in the context of our work in the experimental section.

2. Experimental

2.1 The MSS chip

In the MSS' native state, four beams suspend an otherwise free-floating circular membrane (Fig. 2A) [26,27,29]. The beams are embedded with piezoresistors through boron doping, which are electrically connected to form a Wheatstone bridge circuit. When bridge voltage V_B is supplied to the circuit, the output signal V_{out} varies with the uniaxial stress (transduced as changes in resistance) in the beams.

We use LMBD to deposit a thin DNA film onto the membrane as a receptor material (Fig. 2A). When water adsorbs to the DNA film, its deformation generates surface stress on the membrane, which causes the beams to deflect under uniaxial stress (Fig. 2B)[29]. The uniaxial stress is transduced as relative resistance change $\Delta R_i/R_i$ (i = 1, 2, 3, 4) in the piezoresistors. Resulting V_{out} has been expressed as:

$$V_{out} = \frac{V_B}{4}\left(\frac{\Delta R_1}{R_1} - \frac{\Delta R_2}{R_2} + \frac{\Delta R_3}{R_3} - \frac{\Delta R_4}{R_4}\right)$$

In our experiments, V_{out} is measured through embedded circuits in the MSS and interpreted as sensor output in response to water. Each MSS chip has four such sensing membranes and corresponding readouts (Fig. S1). Membranes can be excluded from the deposition by masking.

The MSS chip used in this study was purchased from NanoWorld AG, Switzerland. Before further processing, the MSS chip was treated with oxygen plasma using a low-pressure plasma system (Femto, version B, Diener Electronic GmbH + Co. KG., Ebhausen, Germany). The plasma power, pressure, and duration were 30 W, 0.50 mbar, and 2 min, respectively.

2.2 LMBD deposition of DNA thin film

DNA sodium salt derived from salmon sperm purchased from MP Bio Japan was dissolved in Ultrapure MilliQ water at a concentration of 10 wt%. A 10 mL petri dish was placed into a cooler padded with dry ice, and the DNA solution was pipetted into it. The DNA solution was left to cool to -78 ℃ over 30 mins to solidify into an ice matrix with embedded DNA. After

solidification, the sample is loaded into the LMBD machine as the deposition target (henceforth referred to as "target").

The LMBD machine was also loaded with the MSS upside down and 120 mm above the deposition target (Fig. 1C). The inside environment was evacuated to 4×10^{-4} Pa using a turbo molecular pump. Under this pressure, the sample sublimates and quickly reaches an equilibrium temperature of -76 ℃, which is maintained during LMBD deposition (elaborated in supplementary materials)[25]. Through a silica glass window, at an angle of 45° to the horizontal, a 532 nm (2nd harmonic of Nd:YAG) laser powered at 620 V was used to irradiate the target. Furthermore, the laser was set up to pass through a focusing lens with a 500 mm focal length, to achieve a spot-size of 1.2 mm at its 415 mm path length to the target. We provided a single pulse of duration 170 μs, measuring 2.7 W, which provides energy to the target.

When the laser energy transfers to the target, the ice sublimates explosively, transitioning from solid phase to gas phase instantly. DNA molecules embedded in the ice matrix are carried by the sublimated water vapor molecules and fly into the MSS positioned above, accumulating into a thin film. The phenomenon is not unlike the desorption of analytes in matrix-assisted laser desorption/ionization (MALDI) used for time-of-flight mass spectroscopy (TOF MS)[3030,31].

As a point of reference for the extent of damage to DNA and its influence on sensor performance, we additionally created a second set of DNA films on MSS using LMBD with a 266 nm (3rd harmonic of Nd:YAG) laser powered at 620 V, with the same focusing lens and duration, measuring 0.3 W. The 266 nm laser is used because it lies in the ultraviolet (UV) range of the electromagnetic spectrum, which is known to be heavily damaging to biological functions, and strongly absorbed by heterocyclic rings in nucleobases.

As a result of this process, the DNA film covers the MSS chip, including its four sensing membranes and circuitry (Fig. S2). The film is not observed to interfere with the electronics of the embedded circuitry and readout pins of the MSS.

2.3 Characterization of DNA film

The surface profile of the LMBD-fabricated DNA thin film was captured using a surface stylus profilometer (Bruker dektak XT) to scan a diameter along the MSS' membrane.

The spectroscopic characteristics were evaluated with Fourier transform infrared spectrophotometry (FT-IR, Nicolet iS20) to determine the degree of damage done to the DNA structure under LMBD processing.

Nucleic acid staining was performed on extracted samples of the DNA films in a 10% polyacrylamide gel with Sybr Gold nucleic acid stain and Tris-glycine buffer to visualize the state of nucleobases after LMBD processing.

2.4 Vapor sensing

To measure sensitivity to water and organic solvents, the MSS with the DNA film receptor was placed in a chamber supplied with headspace vapor from a vial containing the analyte. Initially, pure nitrogen gas is injected at 100 $mLmin^{-1}$ for 300 s to promote desorption of past analytes and thus reset the sensor baseline. Then, pure nitrogen gas flow is reduced to 20 $mLmin^{-1}$, while headspace vapor from the vial is carried into the chamber at 80 $mLmin^{-1}$, keeping the vapor concentration at 80% saturation. This flow is maintained for 300 s while measuring output voltage from the MSS. During measurements, the MSS was supplied with a bridge voltage VB of –0.5 V and recorded at a rate of 20 Hz.

The sensor's response to humidity was also monitored. The mass flowrates of pure nitrogen gas and headspace vapor from a vial containing water are adjusted to simulate a range of 0–90%RH.

3. Results and discussion

3.1 Film thickness/morphology

The LMBD deposition process sublimated a submicrometer-thick layer of DNA material onto the surface of the MSS chip (Fig. 3A). Compared to the distinct coffee-ring pattern in the inkjet-spotted film, the LMBD film has a more stochastic, fluctuating, and noisy profile (Fig. 3B).

The surface profiles of four films were aggregated to calculate the thickness and root-mean-square (RMS) roughness statistics of a typical film fabricated under the conditions prescribed in section 2.2 (Fig. S2).

A typical LMBD film has an average thickness of 0.31 μm with root-mean-square (RMS) roughness of 0.33 μm (Fig. 3C). In comparison, the inkjet-spotted film has an average thickness of 0.53 μm and RMS roughness of 0.71 μm.

From the RMS and surface profile (Fig. 3B) of a typical LMBD film, it is apparent that the films demonstrate high individual variance on the microscale. However, the thickness standard deviation across the four films measured in this study is only 0.05 μm. This low standard deviation indicates a macroscale consistency in morphology contrary to the microscale stochasticity and noisiness.

Thus, LMBD fabrication does not exhibit the same limitations as classic solution-processing fabrication. The distribution of DNA material does not follow evaporation mechanics, instead it is essentially stochastic and noisy on the microscale. However, the microscale stochasticity translates into a macroscale consistency surpassing that of inkjet-spotted DNA films. Such consistency is expected to produce more reproducible sensors with cross-batch consistency in responses.

3.2 Role of DNA hydration in sensor performance

In the MSS sensor, the output voltage V_{out} is transduced from surface stress generated by water adsorbing onto the DNA film. This surface stress is

determined by factors including the film's thickness, its Young's modulus and Poisson ratio, sorption kinetics of water to the film, and the film's viscoelastic behavior[29].

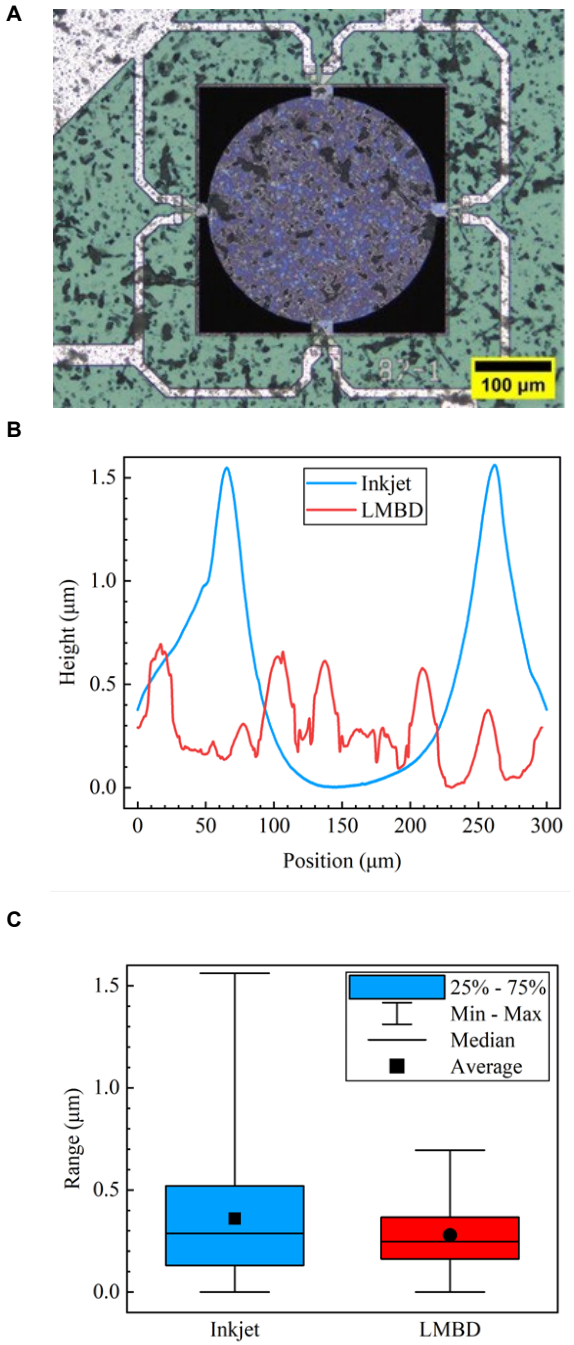


Fig. 3. (A) Microscope image of a single sensing membrane on the MSS with deposited DNA film; See Fig. S2 for images of all four membranes. (B) Thickness profile of the DNA film along the sensing membrane for LMBD compared to inkjet spotting. (C) Statistical distribution of the surface profile of LMBD compared to inkjet spotting; although both films have similar average and median heights, there is significantly more variation in the profile of the inkjet film.

Since the thickness of the DNA film is small compared to the thickness of the sensing membrane (5.2 µm), the film's mechanical properties are not expected to dominate the surface stress[29]. Therefore, sorption kinetics are expected to play a significant role in sensor performance.

It is known that DNA hydration is mediated by water molecules interacting favorably with its structure for several reasons: 1) water, being a polar molecule with a partial positive charge on hydrogen, is electrostatically attracted to the negatively charged phosphate groups in the sugar-phosphate backbone; 2) water can form hydrogen bonds with nucleobases as well as oxygen atoms in the phosphate groups; 3) formation of a hydration shell that stabilizes DNA's helical structure[12].

Since LMBD is typically a process for fabricating thin films of inorganic materials with high melting points, we were concerned that it would be damaging to the DNA structure. This could weaken the ability for DNA to hydrate, and in turn decrease the sorption of water to the DNA film, yielding decreased sensitivity and selectivity of the sensor to water. This was demonstrated in the previous study using LMBD with a continuous IR laser, where signatures associated with the phosphate backbone were essentially diminished following processing[21]. As such, we used Fourier Transform Infrared (FTIR) spectroscopy and nucleic acid staining to determine the nature of structural damage to DNA resulting from the fabrication process and ascertain its effect on interactions with water.

Comparing the FTIR waveforms of LMBD-fabricated to inkjet-spotted DNA film, there are minor changes in peaks 6-11 associated with nucleobases. The nucleobases may have been damaged, but changes in bonding were not sufficiently significant to be apparent on the FTIR waveform.

We also used nucleic acid staining to further assess the damage to nucleobases (Fig. S3). Following laser damage, the nucleic acid stain was still able to bind to the DNA sample from the DNA film created with 532 nm laser. In contrast, in the DNA film created with 266 nm laser, nucleic acid stain failed to bind to the sample. Therefore, there is a significant degree of nucleobase preservation in the DNA film created with 532 nm laser, which could contribute to retention of hydration ability after LMBD-fabrication.

Returning to the FTIR waveform, more significant damage is apparent in the sugar-phosphate backbone, as indicated by the loss of peaks 1 and 2[32]. Particularly, this damage is concentrated in the sugar group, as indicated by a significant reduction in peak 3 associated with C-C and C-O bonds in the deoxyribose, in contrast to the robustness of peak 4 associated with phosphate symmetric stretching[33].

The loss of peak 3 suggesting cleavage of C-C and C-O bonds, coupled with broadening of peak 4 suggesting formation of C=O groups associated with ketones or aldehydes, may indicate the oxidation of

deoxyribose into various carbonyl compounds[34,35]. It is noted that some carbonyl compounds such as 2'-Deoxyribonolactone maintain the integrity of the phosphate group, so their formation may not significantly hinder the hydration behavior of the backbone remnant[34,35].

In contrast, for the DNA film created with the 266 nm laser, the damage is more extensive, encompassing the phosphate groups (Fig. S4). Peaks 3 and 4 are extinguished, and new peaks assignable to ester and carbonyl degradation products appear. In this reference DNA film, both nucleobases and phosphate groups are substantially damaged, so we should expect significantly weaker hydration behavior.

Consequently, it has been observed that the damage LMBD with the 532 nm laser does to DNA is concentrated in the deoxyribose sugar and thus may be minimally inhibitory to hydration of DNA associated with nucleobases and phosphate groups. Therefore, we expect the DNA film fabricated with LMBD at 532 nm to be a valid fabrication approach for a water sensor.

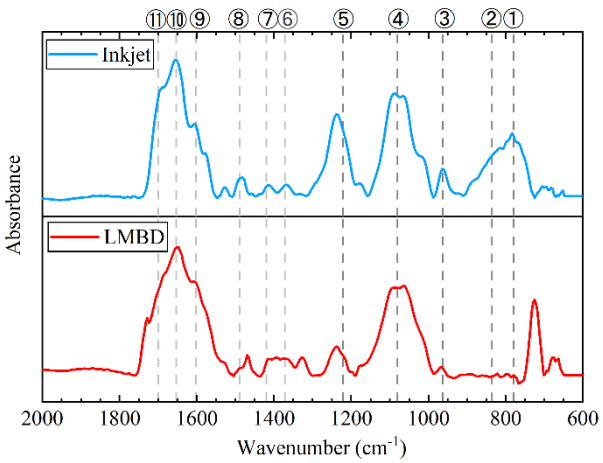


Fig. 4. FTIR spectra of Inkjet- and LMBD-fabricated DNA films. Peaks relevant to sugar phosphate (DNA backbone) are highlighted, and their corresponding band assignments are listed in table 1. The peaks are derived from Gnapareddy et al.'s work[32].

Table 1. Peaks relevant to the chemistry of the sugar phosphate backbone are listed. The table is derived from Gnapareddy et al.'s work [32].

Peak	Wavenumber (cm^{-1})	Band assignment
①	780	Sugar phosphate vibration
②	835	Deoxyribose phosphate
③	963	C-C and C-O of deoxyribose skeletal motion
④	1050~ 1080	Phosphate symmetric stretching
⑤	1221	Phosphate antisymmetric stretching
⑥	1372	Cytosine and Guanine
⑦	1420	Cytosine and Guanine
⑧	1488	Cytosine (in-plane vibration)
⑨	1603	Adenine (C7=N stretching)
⑩	1653	Thymine (C2=O stretching)
⑪	1700	Guanine (C=O stretching)

3.3 Sensor Performance

Despite observable structural damage from LMBD-fabrication, the resulting DNA film maintains very strong interactions with water. This is evident in the high sensitivity and selectivity of the MSS to water compared to organic solvents (Fig. 5A, B).

Across four sensing elements tested in this study, V_{out} of the MSS reaches 25.3 ± 2.6 mV within 0.6 s of exposure to water headspace vapor at 80% saturation (Fig. 5A). This response is approximately 7-22 times that of other organic solvents (Fig. 5B). This large difference in magnitude of responses indicates strong and highly specific interactions between DNA and water; despite other solvents having properties such as hydrophilicity or water-miscibility, they do not interact with DNA in the same capacity as water.

The overall behavior of the current LMBD-fabricated sensor aligns with that of the previously reported inkjet-spotted sensor[14]. However, the magnitude of V_{out} for the inkjet-spotted sensor was 44 mV; it is almost 20 mV higher in magnitude than the current LMBD-fabricated sensor. This drop in magnitude is likely attributable to the structural damage induced by laser energy; hydration was partially

The LMBD-fabricated sensor's response pattern to humidity also aligns with that of the inkjet-spotted sensor. The response increases rapidly between 0-10%RH and begins to gradually increase, saturating at 30%RH (Fig. 5C). At 2%RH, the response is 6 mV; since the theoretical noise of the MSS is ~1 μV and the experimentally observed noise is ~5 μV, the Limit of Detection (LoD) is estimated at 5×10^{-4}%RH. Essentially, the inkjet-spotted sensor with undamaged DNA is three times as sensitive as the LMBD-fabricated sensor.

In the reference DNA film created with 266 nm laser, a slow increase in response between 0-5%RH is observed (Fig. S5). This low response in the low extremities of water concentration makes it nonideal for detecting trace amounts of water. Indeed, the response at 2%RH is 2 mV. Thus, the LoD is estimated as 1.5×10^{-3}%RH. This is significantly less performant than the DNA film created with 532 nm laser. The lower sensitivity of the reference DNA film to water is likely related to the greater destruction of nucleobase and phosphate groups in DNA and resultant weakening in hydration behavior observed during film characterization.

Compared to analogous humidity sensors in literature, the DNA-based MSS in this study exhibits high sensitivity to water (Table S1)[36]. Despite landing second in LoD to our previous work, the remarkable selectivity and sensitivity to water demonstrates a great potential for the detection of trace amounts of water in organic solvents.

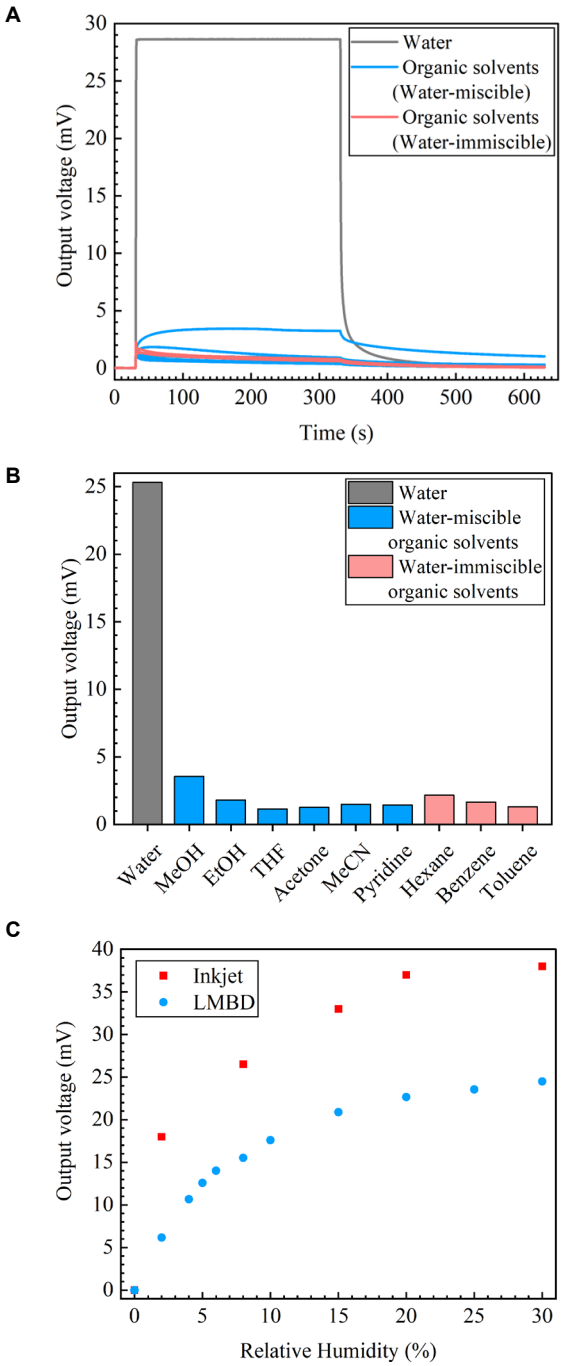


Fig. 5. **(A)** Transduced responses of LMBD-fabricated DNA film to water (black), water-miscible organic solvents (blue), and water-immiscible organic solvents (red) over 300 s of 80% saturated headspace vapors; **(B)** Magnitude of transduced responses showcasing selectivity to water compared to organic solvents; **(C)** Comparison of transduced responses of LMBD-fabricated film compared to inkjet spotted film from previous study.

3.4 Reproducibility of Film and Response

We have described the LMBD-fabricated film as stochastic and noisy on the microscale, as evident from the film profiles (Fig. 3B, Fig. S2). Indeed, we even observe areas on the sensing membrane that are visibly not covered with film material (Fig. S2).

However, the films demonstrate a broadly consistent sensing performance across different films and different fabrication instances, with an average response magnitude of 25.3 ± 2.6 mV across four sensing elements tested in this study (Fig. 6A, B).

This consistency in performance may be related to the macroscale consistency in film morphology, as described in section 3.1. This relationship is reflected in the four films demonstrating an average thickness of 0.31 ± 0.05 µm (Fig. 6B).

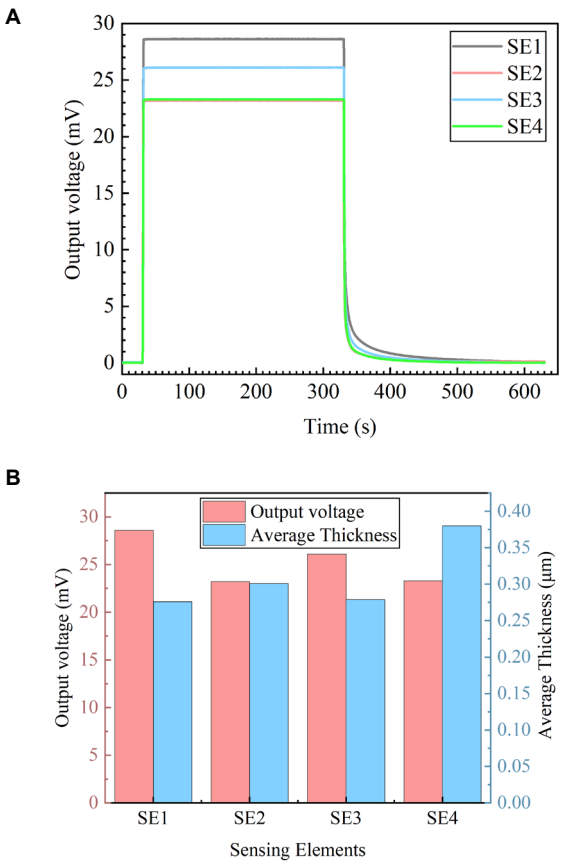


Fig. 6. **(A)** transduced responses to water across four different sensing elements used in this study. **(B)** The magnitude of the response and the average thickness of each film.

3.5 Repeatability of Sensing Response

We tested each sensing element over 10 cycles of injecting 20 $mLmin^{-1}$ nitrogen and 80 $mLmin^{-1}$ water vapor. The drift in magnitude of the transduced response over the 10 cycles and statistical distribution thereof is plotted and shown in supplementary materials (Fig. S6).

One sensing element denoted SE1 is shown in Fig. 7A as an example. The average magnitude of the transduced response in SE1 over 10 cycles was 28.6 ± 0.5 mV (Fig. 7B). The low standard deviation of only 1.7% of the average indicates a stable, repeatable performance. Similarly repeatable performance can be found in SE2, SE3, and SE4 (Fig. S6).

4. Conclusion

We fabricated sub-micrometer thick films of DNA using LMBD processing with a pulsed 532 nm laser. The purpose of this study was to explore the use of LMBD processing as a more well-controlled fabrication process for the high sensitivity and selectivity water sensor reported previously, which had limited reproducibility due to between-batch differences arising from the inkjet-spotting solution processing fabrication approach.

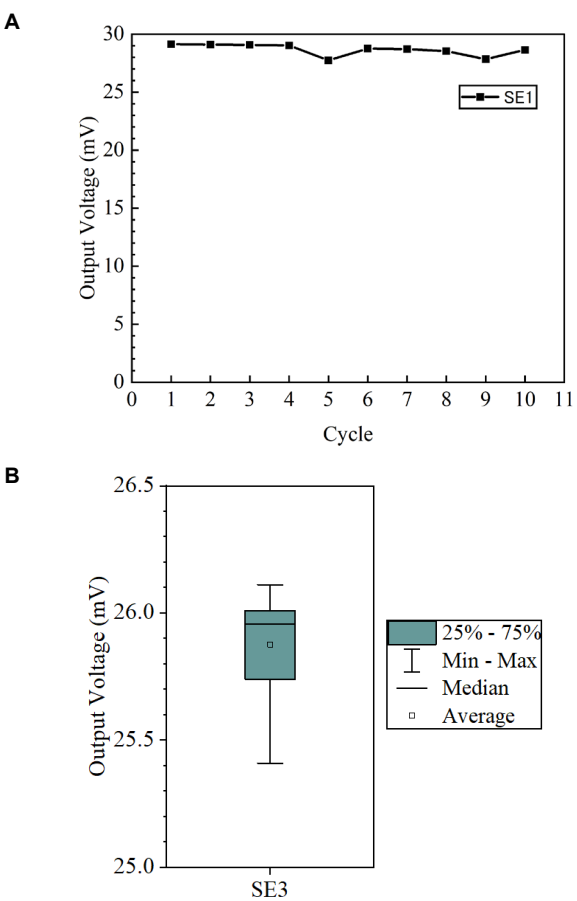


Fig. 7. (A) Magnitude of transduced response to water for a single sensing element over 10 cycles of injecting 80 $mLmin^{-1}$ water vapor. **(B)** Statistical distribution of magnitude of transduced response over 10 cycles.

The LMBD-fabricated film has significantly lower thickness compared to the inkjet-spotted film. At an average thickness of 0.31 μm with RMS roughness of 0.33 μm, the film distribution is highly stochastic and rough on the microscale, but this stochastic conformation translates into a macroscale reproducibility exceeding that of inkjet-spotted films.

Since the film is thin and soft relative to the sensing membrane, changes to sorption kinetics due to DNA damage during LMBD would dominate sensing performance differences to inkjet-spotted films. We compared FTIR spectra and nucleic acid staining of the LMBD film to pristine DNA to evaluate and characterize damage done to DNA during fabrication. From changes in spectral signatures, it is likely that damage was concentrated in the deoxyribose sugars and is oxidative in nature. Since the phosphate groups and nucleobases retain ability to electrostatically attract water and form hydrogen bonds, the DNA material maintains strong interactions with water. Thus, we expected LMBD to be a valid fabrication approach for water-sensing DNA films.

Next, we evaluate the sensor performance. The magnitude of the sensor's response is 25.3 ± 2.6 mV. Although this response is less compared to the inkjet-spotted sensor, it retains high selectivity because the response to water is 7-22 times that of the response to organic solvents, regardless of their hydrophilicity or water-miscibility. The sensor retains high sensitivity in the lower extremities of water concentration; the LoD was determined to be 5×10^{-4}%RH. While three times weaker than the inkjet-spotted sensor, this performance remains competitive with the best humidity sensors in literature.

The sensor's performance is reproducible, as response times and magnitude of the transduced response is shown to be consistent across four different sensing elements. This reproducibility indicates a macroscale consistency in film morphology, which is further evidenced by the average thickness of the films having low standard deviation. Each sensing element is also shown to remain stable with minimal drift over 10 cycles of injecting water vapor.

In general, the magnitude of the sensor's response to water is lower compared to the previously reported inkjet spotting solution-processed sensor. This is likely due to structural damage caused by the high-energy nature of the LMBD fabrication approach in the current study. However, the selectivity to water over organic solvents remains very high, so its application for detecting trace amounts of water in organic solvents remains valid. Furthermore, LMBD processing is a well-controlled fabrication process that is more suited for large-scale fabrication of consistent batches.

In future work, optimization of LMBD parameters could enhance the performance of the MSS device, yielding incremental improvements in performance. This could result in a commercial device that could reproducibly, repeatably, and universally detect trace amounts of water in organic solvents, providing a more convenient alternative to KF titration.

Funding

This work was supported by a grant from the Kanagawa University Engineering Research Institute, Collaborative Research A and JST SPRING, Grant Number JPMJSP2108. This study was supported by Japan Society for the Promotion of Science KAKENHI, Grant Numbers JP25H00898 and JP23H05459

Conflict of interest statement. None declared.

References

1. Isengard, H. Rapid water determination in foodstuffs. *Trends Food Sci. Technol.* **6**, 155–162 (1995).
2. Rivera-quintero, P. *et al.* Experimental methods in chemical engineering : Karl Fischer titration. *Can. J. Chem. Eng.* **102**, 2980–2997 (2024).
3. Larsson, W., Jalbert, J., Gilbert, R. & Cedergren, A. Efficiency of Methods for Karl Fischer Determination of Water in Oils Based on Oven Evaporation and Azeotropic Distillation. *Anal. Chem.* **75**, 1227–1232 (2003).
4. Margolis, S. A. Sources of Systematic Bias in the Measurement of Water by the Coulometric and Volumetric Karl Fischer Methods. *Anal. Chem.* **69**, 4864–4871 (1997).
5. Yola, Y. & Fischer, K. Automation of Karl Fischer Water Titration by Flow Injection Sampling. *Anal. Chem.* **62**, 2504–2506 (1990).
6. Jung, H. S., Verwilst, P., Kim, W. Y. & Kim, J. S. Chem Soc Rev Fluorescent and colorimetric sensors for the detection of humidity or water content. *Chem. Soc. Rev.* **45**, 1242–1256 (2016).
7. Jouyban, A. & Rahimpour, E. Optical sensors for determination of water in the organic solvents : a review. *J. Iran. Chem. Soc.* **19**, 1–22 (2022).
8. Qi, H., Liu, J., Deng, Y., Gao, S. & Mader, E. Cellulose fibres with carbon nanotube networks for water sensing. *J. Mater. Chem. A* **2**, 5541–5547 (2014).
9. Kang, E. *et al.* A simple method to determine the water content in organic solvents using the 1 H NMR chemical shifts differences between water and solvent. *Microchem. J.* **138**, 395–400 (2018).
10. Singh, A. K., Wen, C., Cheng, S. & Vinh, N. Q. Long-range DNA-water interactions. *Biophys. J.* **120**, 4966–4979 (2021).
11. Satange, R. & Hou, M. Chemical Biology The role of water in mediating DNA structures. *RSC Chem. Biol.* **6**, 699–720 (2025).
12. Duboue, E., Fogarty, A. C., Hynes, J. T. & Laage, D. Dynamical Disorder in the DNA Hydration Shell. *J. Am. Chem. Soc.* **138**, 7610–7620 (2016).
13. Dom, C. M. *et al.* Hydration Induced Stress on DNA Monolayers Grafted on Microcantilevers. *Langmuir* **30**, 10962–10969 (2014).
14. Murata, T., Minami, K., Yamazaki, T., Yoshikawa, G. & Ariga, K. Detection of Trace Amounts of Water in Organic Solvents by DNA-Based Nanomechanical Sensors. *Biosensors* **12**, (2022).
15. Seo, C., Jang, D., Chae, J. & Shin, S. Altering the coffee-ring effect by adding a surfactant-like viscous polymer solution. *Sci. Rep.* 1–9 (2017) doi:10.1038/s41598-017-00497-x.
16. Shimobayashi, S. F., Tsudome, M. & Kurimura, T. Suppression of the coffee-ring effect by sugar-assisted depinning of contact line. *Sci. Rep.* **8**, 1–9 (2018).
17. Okaiyeto, S. A., Xiao, H. & Mujumdar, A. S. Understanding the coffee ring effect : how it has led to advanced applications. *Dry. Technol.* **41**, 1083–1084 (2023).
18. Nikolov, A. D., Wasan, D. T. & Wu, P. ScienceDirect Marangoni flow alters wetting : Coffee ring and superspreading. *Curr. Opin. Colloid Interface Sci.* **51**, 101387 (2021).
19. Hu, H. & Larson, R. G. Marangoni Effect Reverses Coffee-Ring Depositions. 7090–7094 (2006).
20. He, P. & Derby, B. Controlling Coffee Ring Formation during Drying of Inkjet Printed 2D Inks. **1700944**, 2–7 (2017).
21. Murata, T. *et al.* Nanometer-Flat DNA-Featured Thin Films Prepared via Laser Molecular Beam Deposition under High-Vacuum for Selective Methanol Sensing. *Bull. Chem. Soc. Jpn.* **96**, 29–34 (2023).
22. Eason, R. *Pulsed Laser Deposition of Thin Films: Applications-Led Growth of Functional Materials*. (2006).
23. Popescu, C. & Dorcioman, Gabriela Popescu, A. Laser Ablation Applied for Synthesis of Thin Films: Insights into Laser Deposition Methods. in *Applications Of Laser Ablation - Thin Film Deposition, Nanomaterial Synthesis And Surface Modification* 3–32 (2016).
24. Aziz, M. J. Film growth mechanisms in pulsed laser deposition. 579–587 (2008) doi:10.1007/s00339-008-4696-7.
25. Khairnar, S., Kini, R., Harwalkar, M., Salunkhe, K. & S.R., C. A Review on Freeze Drying Process of Pharmaceuticals. *Int. J. Res. Pharm. Sc.* **4**, 76–94 (2013).
26. Loizeau, F. *et al.* Piezoresistive membrane-type surface stress sensor arranged in arrays for cancer diagnosis through breath analysis. *Proc. IEEE Int. Conf. Micro Electro Mech. Syst.* **1**, 621–624 (2013).
27. Yoshikawa, G., Akiyama, T., Gautsch, S., Vettiger, P. & Rohrer, H. Nanomechanical Membrane-type Surface Stress Sensor. 1044–1048 (2011).
28. Albert, K. J. *et al.* Cross-Reactive Chemical Sensor Arrays. *Chem. Rev.* **100**, 2595–2626 (2000).
29. Minami, K., Imamura, G., Tamura, R., Shiba, K. & Yoshikawa, G. Recent Advances in Nanomechanical Membrane-Type Surface Stress Sensors towards Artificial Olfaction. *Biosensors* **12**, 1–34 (2022).
30. Wu, K. J., Shaler, T. A. & Becker, C. H. Time-of-Flight Mass Spectrometry of Underivatized Single-Stranded DNA Oligomers by Matrix-Assisted Laser Desorption. *Anal. Chem.* **66**, 1637–1645 (1994).
31. Strasse, R., Gross, J. & Strupat, K. Matrix-assisted laser desorption / ionisation ^ mass spectrometry applied to biological macromolecules. *Trends Anal. Chem.* **17**, 470–484 (1998).
32. Gnapareddy, B., Dugasani, S. R., Ha, T. & Paulson, B. Chemical and Physical Characteristics of Doxorubicin Hydrochloride Drug-Doped Salmon. *Nat. Publ. Gr.* 1–9 (2015) doi:10.1038/srep12722.
33. Suzuki, T. Review DNA Damage and Mutation Caused by Vital Biomolecules , Water , Nitric Oxide , and Hypochlorous Acid. **28**, 48–55 (2006).
34. Nakamura, J. & Nakamura, M. DNA-protein crosslink formation by endogenous aldehydes and AP sites. *DNA Repair (Amst).* **88**, 102806 (2020).
35. Chan, S. W. & Dedon, P. C. The Biological and Metabolic Fates of Endogenous DNA Damage Products. **2010**, (2010).

36. Mistry, K. *et al.* Highly Sensitive Self-Actuated Zinc Oxide Resonant Microcantilever Humidity Sensor. *Nano Lett.* **22**, 3196–3203 (2022).